Mainz preprint KOMA-96-19
May/December 1996

Monte Carlo Study of Pure-Phase Cumulants of 2D q-State Potts Models

Wolfhard Janke and *Stefan Kappler*

Institut für Physik, Johannes Gutenberg-Universität Mainz,
Staudinger Weg 7, 55099 Mainz, Germany

Abstract

We performed Monte Carlo simulations of the two-dimensional q-state Potts model with $q = 10$, 15, and 20 to study the energy and magnetization cumulants in the ordered and disordered phase at the first-order transition point β_t. By using very large systems of size 300×300, 120×120, and 80×80 for $q = 10$, 15, and 20, respectively, our numerical estimates provide practically (up to unavoidable, but very small statistical errors) exact results which can serve as a useful test of recent resummed large-q expansions for the energy cumulants by Bhattacharya *et al.* [J. Phys. I (France) **7** (1997) 81]. Up to the third order cumulant and down to $q = 10$ we obtain very good agreement, and also the higher-order estimates are found to be compatible.

PACS numbers: 02.70.Lq, 64.60.Cn, 75.10.Hk

To appear in *J. Phys. I (France), May 1997*

1 Introduction

A detailed understanding of first-order phase transitions plays an important role in many fields of physics [1]. In particular the finite-size scaling behaviour near the transition has been a subject of increasing interest in recent years [2]. It is well known, and in limiting cases exactly proven [3], that thermodynamic observables in equilibrium can be expanded as asymptotic power series in $1/V$, where V is the volume of the system. The range of applicability of such expansions, however, is widely unknown and was the source for quite a few apparent inconsistencies in the recent literature. As has been discussed in a recent series of papers by Bhattacharya *et al.* [4–8], a precise knowledge of the energy cumulants of the coexisting phases at the transition point β_t in the infinite-volume limit can help to understand and to resolve these problems.

The explicit calculations by Bhattacharya *et al.* have been performed for the two-dimensional (2D) q-state Potts model [9, 10], which for $q \geq 5$ is the paradigm for a system with a temperature-driven first-order phase transition. The advantage of this model is that many properties (transition point β_t [11], internal energy [11] and magnetization [12] of the pure phases at β_t, correlation length [13] and interface tension [14] at β_t) are exactly known and that the parameter q (the number of states per spin) allows one to tune the strength of the transition. Based on the Fortuin-Kasteleyn representation [10, 15] of the Potts model, Bhattacharya *et al.* analyzed the ensuing clusters to obtain large-q series expansions for the energy cumulants in the ordered phase at β_t and then applied Padé-type resummations to arrive at numerical estimates.

Since, as with every resummed series expansion, it is intrinsically difficult to provide reliable estimates of the size of systematic errors, we found it worthwhile to determine the cumulants by a completely independent method, namely Monte Carlo simulations. For large enough system sizes the systematic errors are negligible (of the order $\exp(-L/\xi)$, where L is the linear size of the system and ξ the finite correlation length), and by increasing the simulation time also the statistical errors can be made as small as desired. In the following we report high-statistics measurements of the first ten energy cumulants in the ordered and disordered phase at β_t for the models with $q = 10$, 15, and 20. With increasing order we observe the expected steep growth of the energy cumulants. The accuracy of the estimates, however, decreases with increasing order because the tail ends of the energy distribution become

more and more important. Up to the third-order cumulant the precision of the numerical estimates is still high (about 1% or better), and we obtain very good agreement with the large-q expansions down to $q = 10$. At fourth order the agreement between the two methods is still good within the statistical error bounds of about $5\% - 15\%$, and also the results for the fifth and sixth order, the highest energy cumulants considered in Ref. [8], are compatible with each other. The further estimates up to the tenth order should only be taken as a rough indication of the order of magnitude in high orders of the cumulant expansion. In addition we also present estimates of the first three magnetization cumulants in the two phases at β_t, and compare the susceptibility in the ordered phase with recent low-temperature series expansions for $q = 10$.

The remainder of the paper is organized as follows. In Sec. 2 we first briefly recall the model and some exact results. We then describe the set-up of our simulations and discuss the estimators used for measuring the various cumulants. The numerical data are presented in Sec. 3, and in Sec. 4 we conclude with a brief summary of the main results and a few final remarks.

2 Model and simulation

In our simulations we employed the standard definition of the Potts model partition function [9, 10]

$$Z = e^{-\beta F} = \sum_{\{s_i\}} e^{-\beta E};\; E = -\sum_{\langle ij \rangle} \delta_{s_i s_j};\; s_i = 1, \ldots, q, \tag{1}$$

where $\beta = J/k_B T$ is the inverse temperature in natural units, F is the free energy, i denote the sites of a two-dimensional square lattice, $\langle ij \rangle$ are nearest-neighbor pairs, and $\delta_{s_i s_j}$ is the Kronecker delta symbol.

All simulations were performed in the canonical ensemble at $\beta = \beta_t = \ln(1 + \sqrt{q})$, employing large square lattices of size 300×300, 120×120, and 80×80 for $q = 10$, 15, and 20, respectively, and periodic boundary conditions. To stabilize the pure ordered or disordered phase we took advantage of the extremely small tunneling probability for large system sizes [16–19]. Since the tunneling proceeds via mixed phase configurations with two interfaces, the probability is proportional to $\exp(-2\sigma_{od} L)$, where σ_{od} is the interface tension between the ordered and disordered phase. For 2D Potts models

σ_{od} has been analytically predicted [14], $2\sigma_{od} = 1/\xi_d(\beta_t)$, where $\xi_d(\beta_t)$ is the exactly known [13] correlation length in the disordered phase at the transition point ($= 10.559519\ldots$, $4.180954\ldots$, and $2.695502\ldots$ for $q = 10$, 15, and 20). By rewriting the tunneling probability as $\exp(-L/\xi_d)$, it is easy to estimate that for our choice of lattice sizes, $L \approx 28\xi_d$, the order of magnitude is about $\exp(-28) \approx 10^{-12}$. It is therefore extremely probable that, starting from a completely ordered or disordered configuration, the system will stay in the ordered or disordered phase during a very long (but finite) simulation time, thereby allowing statistically meaningful pure-phase measurements of energy and magnetization cumulants. To be sure we have of course monitored the time evolution of our simulations and explicitly verified that no tunnelings occurred. In Fig. 1 we show the probability distributions $P(e)$ of the energy density $e = E/V$ in the ordered as well as in the disordered phase, demonstrating that the two peaks are indeed very well separated.

The finite-size corrections in the pure phases are also expected to be of the order $\exp(-L/\xi_p)$, where the subscript p stands for the ordered (o) and disordered (d) phase, respectively. Since we have recently obtained strong numerical evidence that $\xi_o(\beta_t) = \xi_d(\beta_t)$ [18, 19], this yields for the chosen lattice sizes in both phases again an order of magnitude estimate of $\exp(-28) \approx 10^{-12}$.

To update the spins we employed in the ordered phase the heat-bath algorithm, while in the disordered phase it is more efficient to use the single-cluster algorithm [16, 17]. The observed integrated autocorrelation times of the energy, $\tau_{\mathrm{int},e}$, and the statistics parameters are compiled in Table 1. Notice that for the heat-bath algorithm $\tau_{\mathrm{int},e}$ scales roughly with ξ_o^2, as one would have expected on general grounds. For the single-cluster algorithm we followed the usual convention and defined $V/\langle|C|\rangle_{d,\mathrm{SC}}$ single-cluster steps as one Monte Carlo update sweep (MCS), where $\langle|C|\rangle_{d,\mathrm{SC}}$ is the average cluster size (cf. Table 5 below).

The simulations with the heat-bath algorithm were performed on a CRAY vector computer. To estimate statistical errors we divided the runs into several bins and employed the standard jack-knife procedure. The single-cluster code was implemented on a T3D parallel computer by simulating 64 time histories in parallel. This enabled us to gather an equivalent of about five workstation CPU years within a relatively short time. Here the error bars are estimated from the fluctuations between the 64 copies by using again the jack-knife procedure.

The primary observables we report here are the energy cumulants $\kappa_p^{(n)}(\beta_t)$ at the transition point $\beta_t = \ln(1+\sqrt{q})$, which are defined through the Taylor expansion of the scaled free energy density $\beta f = \beta F/V$ around $\beta = \beta_t$,

$$-\beta f_p(\beta) = -\beta_t f(\beta_t) + \sum_{n=1} (-1)^n \kappa_p^{(n)}(\beta_t)(\beta - \beta_t)^n/n! \,. \tag{2}$$

While the free energy is continuous at a first-order phase transition, $f(\beta_t) = f_o(\beta_t) = f_d(\beta_t)$, the cumulants are discontinuous and hence different in the ordered and disordered phase. The first three cumulants coincide with the (central) moments,

$$\begin{aligned}
\kappa_p^{(1)} &= e_p = \langle E \rangle_p / V, & (3)\\
\kappa_p^{(2)} &= c_p/\beta_t^2 = \mu_p^{(2)} = (\langle E^2 \rangle_p - \langle E \rangle_p^2)/V, & (4)\\
\kappa_p^{(3)} &= \mu_p^{(3)} = \langle (E - \langle E \rangle_p)^3 \rangle_p / V, & (5)
\end{aligned}$$

where c_p is the usual specific heat in the pure phases. The higher-order cumulants can be expressed as non-linear combinations of the central moments $\mu_p^{(n)} = \langle (E - \langle E \rangle_p)^n \rangle_p / V$, e.g.,

$$\begin{aligned}
\kappa_p^{(4)} &= \mu_p^{(4)} - 3V {\mu_p^{(2)}}^2, & (6)\\
\kappa_p^{(5)} &= \mu_p^{(5)} - 10V \mu_p^{(2)} \mu_p^{(3)}, & (7)\\
\kappa_p^{(6)} &= \mu_p^{(6)} - 15V \mu_p^{(2)} \mu_p^{(4)} - 10V {\mu_p^{(3)}}^2 + 30V^2 {\mu_p^{(2)}}^3, & (8)
\end{aligned}$$

and so on as listed up to the tenth order in the Appendix. While at β_t both e_o and e_d are known exactly [11], the energy cumulants $\kappa_o^{(n)}$ and $\kappa_d^{(n)}$ with $n \geq 2$ can only be related to each other via duality [10]. In particular for c_o and c_d as well as $\mu_o^{(3)}$ and $\mu_d^{(3)}$ the duality relations read

$$\begin{aligned}
c_o &= c_d - \beta_t^2 (e_d - e_o)/\sqrt{q}, & (9)\\
\mu_o^{(3)} &= -\mu_d^{(3)} + 2(1-q)/q^{3/2} - 3(e_d - e_o)/q + 6c_d/(\beta_t^2 \sqrt{q}). & (10)
\end{aligned}$$

For the magnetization cumulants we have used slightly different definitions in the ordered and disordered phase. In the disordered phase the magnetization vanishes and the magnetic susceptibility can be defined as

$$\chi_d = \frac{1}{V(q-1)^2} \langle \left(\sum_i (q\delta_{s_i,s} - 1) \right)^2 \rangle_d, \tag{11}$$

which is certainly independent of the choice of the reference orientation $s = 1, \ldots, q$. In simulations employing cluster-update algorithms the same quantity can also be estimated from

$$\chi_d = \frac{1}{q-1}\langle |C| \rangle_{d,\mathrm{SC}} = \frac{1}{q-1}\frac{\langle |C|^2 \rangle_{d,\mathrm{SW}}}{\langle |C| \rangle_{d,\mathrm{SW}}}, \tag{12}$$

where $|C|$ denotes the size or weight of a cluster, i.e., the number of spins belonging to a cluster, and the subscripts "SC" and "SW" refer to averages over the clusters encountered in the single-cluster and Swendsen-Wang formulation, respectively. Alternatively one could also measure the (projected) spin-spin correlation function $g(i)$, using the spin or one of the cluster representations, and derive χ_d as the "integral" of $g(i)$, $\chi_d = (q/(q-1)^2)\sum_i g(i)$ [16, 17].

In the ordered phase we have measured the maximum definition of the magnetization

$$M_{\max} = \frac{qN_{\max} - V}{q-1}; \quad N_{\max} = \max\{N_1, N_2, \ldots, N_q\}, \tag{13}$$

where N_s counts the number of spins of orientation $s = 1, \ldots, q$ in a given configuration. A cluster estimator for the magnetization is

$$M_{\mathrm{clus}} = |C_{\max}|, \tag{14}$$

where $|C_{\max}|$ denotes the size of the largest (spanning) stochastic cluster in each spin configuration. The expectation values $m = \langle M_{\max} \rangle_o / V$ and $m' = \langle M_{\mathrm{clus}} \rangle_o / V$ coincide, $m = m'$, and can be directly compared with the exact result for $q \geq 5$, $m = \prod_{n=1}^{\infty} [(1-x^n)/(1-x^{4n})]$, with $0 < x < 1$ defined by $q = x + 2 + x^{-1}$ [12]. The magnetic susceptibility in the ordered phase is computed as

$$\chi_o = \left(\langle M_{\max}^2 \rangle_o - \langle M_{\max} \rangle_o^2 \right) / V, \tag{15}$$

and the third-order magnetization cumulant (or central moment) is given by

$$m_o^{(3)} = \langle (M_{\max} - \langle M_{\max} \rangle_o)^3 \rangle_o / V. \tag{16}$$

Notice that while the expectation values of $M_{\max}$ and M_{clus} coincide, this is not the case for the susceptibilities χ_o and χ'_o, where the latter is defined by (15) with $M_{\max}$ replaced by M_{clus}. The same remark applies of course also to the third-order cumulants $m_o^{(3)}$ and $m'^{(3)}_o$.

3 Results

The Monte Carlo results for e_p, c_p, and $\mu_p^{(3)}$ at β_t are collected in Table 2 ($p = d$, disordered phase) and Table 3 ($p = o$, ordered phase). For comparison we have also listed previous measurements [17, 19] on smaller lattices which clearly demonstrate that the above described "dynamically stabilized" pure phase simulations are feasible and that, as expected, the residual finite-size corrections are completely covered by the statistical errors.

The Table 2 shows the Monte Carlo results for the first three energy cumulants at β_t obtained from the simulations in the disordered phase. The first moments, e_d, are in excellent agreement with the exact results, with relative statistical errors of the order 2×10^{-5}. This indicates quantitatively that systematic errors are completely under control (including possible problems with pseudo-random numbers). The lines denoted by "(large q)" show for the readers convenience the duality transformed estimates from the large-q expansions for the cumulants in the ordered phase (cp. Table 3). To be specific, for $\mu_d^{(3)}$ we have rewritten (10) with the help of (9) as $\mu_d^{(3)} = -\mu_o^{(3)} + 2(1-q)/q^{3/2} + 3(e_d - e_o)/q + 6c_o/(\beta_t^2\sqrt{q})$ and inserted the large-q estimates of Table 3, which are taken from the most recent publication [8].

In Table 3 we show the first three energy cumulants at β_t in the ordered phase obtained first directly from the simulations in the ordered phase (denoted by, e.g., (o, $L \times L$)), and second via the duality relations (9) and (10) using the just described results in the disordered phase (denoted by, e.g., (d, $L \times L$)) collected in Table 2. Also in the ordered phase the exactly known first moments are confirmed with high precision, and the duality relations are very well satisfied by the two independent sets of Monte Carlo simulations, which further underlines the reliability of the data. As already mentioned above, the large-q expansion estimates are taken from Ref. [8]. (Thanks to longer series expansions and constantly improved analysis techniques the numbers given in [4–8] scatter a little bit, reflecting the current state of the art.) We see that in all cases the agreement between the Monte Carlo and large-q estimates is extremely good. The only exception is perhaps $\mu_d^{(3)}$ for $q = 10$, but here quite naturally the systematic error of the large-q expansion is already relatively large. Recent analyses of low- and high-temperature series expansions for the $q = 10$ Potts model specific heat at β_t, on the other

hand, yielded much larger values of $c_o = 31.8(2.8)$ and $c_d = 33(3)$ [20].

For the $2L \times L$ and $2L \times 2L$ lattices we have also computed higher-order energy moments and the resulting cumulants. Our results up to the eighth order are collected in Table 4. With increasing order these observables become very sensitive to the tail ends of the energy distribution and the statistical accuracy deteriorates quite rapidly. Due to cancellation effects this decrease in accuracy is much more pronounced for the cumulants than for the (central) moments. For $\kappa_p^{(4)}$ the statistical errors are about $5\% - 15\%$, and here we still find quantitative agreement of $\kappa_o^{(4)}$ with the resummed large-q expansions, whose estimated systematic errors are of the same order. Also for $\kappa_o^{(5)}$ and $\kappa_o^{(6)}$ the agreement with the results read off from Fig. 13 of Ref. [8] is quite satisfactorily, even though the statistical errors are obviously already quite large. For $\kappa_p^{(7)}$ and $\kappa_p^{(8)}$ some entries in Table 4 are no longer reliable and only the orders of magnitude should be trusted. Here we have certainly reached the limit of the present simulations, in particular for $q = 10$, and just as a very rough estimate we finally quote $\kappa_o^{(9)} \approx 10^{23}$, 10^{19}, and 10^{16}, and $\kappa_o^{(10)} \approx 10^{27}$, 10^{22}, and 10^{19}, for $q = 10$, 15, and 20, respectively. As an example we show in Fig. 2 for $q = 10$ the cumulant expansion around β_t of the energy density $e = -(d/d\beta)(-\beta f)$ in the disordered phase and compare the results with extrapolations obtained by the standard reweighting method.

The Table 5 collects the expectation values for the susceptibility χ_d at β_t, using the two different cluster estimators (12). For comparison we have also included the integral over the zero-momentum correlation function $g(i)$ [16, 17], which was also computed by employing a Swendsen-Wang cluster estimator. One can show that this amounts only to a different implementation of precisely the same operations needed to compute directly the Swendsen-Wang cluster estimator in eq. (12), and therefore the first and second lines for each lattice size in Table 5 in fact turn out to be identical as they should.

The results in Table 6 for the magnetization in the ordered phase clearly confirm that $m = m'$ with high precision. About 5-6 significant digits of the numerical estimates agree within their 1σ error bounds with the exact results of Ref. [12], which provides further evidence that all measured numbers can be interpreted as pure phase expectation values. Furthermore we note that as expected the higher moments of $M_{\max}$ and M_{clus} do not agree. More quantitatively we find consistently that $\chi_o > \chi'_o$ and $|m_o^{(3)}| > |m'^{(3)}_o|$. The proper susceptibility χ_o for $q = 10$ has also been considered in the low-

temperature series analysis of Briggs *et al.* (BEG) [20]. They obtained an estimate of $\chi(\beta_t^+)_{\rm BEG} = 2.44(9)$, leading to $\chi_o = (\frac{q}{q-1})^2 \chi(\beta_t^+)_{\rm BEG} = 3.01(12)$, which is significantly smaller than our value of 4.744(42) on the 300×300 lattice.

4 Summary

We have performed high-precision Monte Carlo simulations in the ordered and disordered phase of 2D q-state Potts models with $q = 10$, 15, and 20 at their first-order transition point, working with large lattices of linear size $L \approx 28\xi_d$ ($= 300$, 120, 80). As an important self-consistency test the first three energy cumulants are found to satisfy the duality relations with high precision, and both the energy and the magnetization are fully consistent with Baxter's exact values. As our main result we obtain for the first three energy cumulants very good agreement with recent resummed large-q expansions of Bhattacharya *et al.* [8], indicating that their technique can give reliable results at least down to $q = 10$. Also the fourth- to sixth-order cumulants are found in reasonably good agreement, albeit the accuracy of both methods decreases with increasing order. We find, however, significant differences to low- and high-temperature series analyses of the specific heat and magnetic susceptibility of the $q = 10$ Potts model at β_t.

Acknowledgements

WJ thanks the DFG for a Heisenberg fellowship and SK gratefully acknowledges a fellowship by the Graduiertenkolleg "Physik and Chemie supramolekularer Systeme". Work supported by computer grants hkf001 of HLRZ Jülich and bvpf03 of Norddeutscher Vektorrechnerverbund (NVV) Berlin-Hannover-Kiel.

Appendix

This appendix lists the relation between cumulants and central moments. To simplify the notation we employ here the definitions $\kappa_n = V\kappa_p^{(n)}$ and $\mu_n = V\mu_p^{(n)} = \langle (E - \langle E \rangle_p)^n \rangle_p$. With the help of computer algebra we obtained

$$
\begin{aligned}
\kappa_4 &= \mu_4 - 3\mu_2^2, \\
\kappa_5 &= \mu_5 - 10\mu_2\mu_3, \\
\kappa_6 &= \mu_6 - 15\mu_2\mu_4 - 10\mu_3^2 + 30\mu_2^3, \\
\kappa_7 &= \mu_7 - 21\mu_2\mu_5 - 35\mu_3\mu_4 + 210\mu_3\mu_2^2, \\
\kappa_8 &= \mu_8 - 28\mu_2\mu_6 - 56\mu_3\mu_5 + 420\mu_4\mu_2^2 - 35\mu_4^2 + 560\mu_3^2\mu_2 - 630\mu_2^4, \\
\kappa_9 &= \mu_9 - 36\mu_2\mu_7 - 84\mu_3\mu_6 - 126\mu_4\mu_5 + 756\mu_5\mu_2^2 \\
&\quad + 2520\mu_2\mu_3\mu_4 + 560\mu_3^3 - 7560\mu_3\mu_2^3, \\
\kappa_{10} &= \mu_{10} - 45\mu_2\mu_8 - 120\mu_3\mu_7 - 210\mu_4\mu_6 - 126\mu_5^2 \\
&\quad + 1260\mu_6\mu_2^2 + 5040\mu_2\mu_3\mu_5 + 3150\mu_4^2\mu_2 + 4200\mu_4\mu_3^2 \\
&\quad - 18900\mu_4\mu_2^3 - 37800\mu_3^2\mu_2^2 + 22680\mu_2^5.
\end{aligned}
$$

References

[1] *Dynamics of First Order Phase Transitions*, eds. H.J. Herrmann, W. Janke, and F. Karsch (World Scientific, Singapore, 1992); K. Binder, Rep. Prog. Phys. **50** (1987) 783; J.D. Gunton, M.S. Miguel, and P.S. Sahni, in *Phase Transitions and Critical Phenomena*, Vol. 8, eds. C. Domb and J.L. Lebowitz (Academic Press, New York, 1983).

[2] For recent reviews see, e.g., A. Billoire, Nucl. Phys. **B** (Proc. Suppl.) **42** (1995) 21; W. Janke, in *Computer Simulations in Condensed Matter Physics VII*, eds. D.P. Landau, K.K. Mon, and H.B. Schüttler (Springer Verlag, Heidelberg, Berlin, 1994); p. 29; and references therein.

[3] C. Borgs, R. Kotecký, and S. Miracle-Solé, J. Stat. Phys. **62** (1991) 529; C. Borgs and R. Kotecký, J. Stat. Phys. **61** (1990) 79;

[4] T. Bhattacharya, R. Lacaze, and A. Morel, Europhys. Lett. **23** (1993) 547.

[5] T. Bhattacharya, R. Lacaze, and A. Morel, Nucl. Phys. **B** (Proc. Suppl.) **34** (1994) 671.

[6] T. Bhattacharya, R. Lacaze, and A. Morel, Nucl. Phys. **B435** (1995) 526.

[7] T. Bhattacharya, R. Lacaze, and A. Morel, Nucl. Phys. **B** (Proc. Suppl.) **42** (1995) 743.

[8] T. Bhattacharya, R. Lacaze, and A. Morel, J. Phys. I (France) **7** (1997) 81.

[9] R.B. Potts, Proc. Camb. Phil. Soc. **48** (1952) 106.

[10] F.Y. Wu, Rev. Mod. Phys. **54** (1982) 235; *ibid.* **55** (1983) 315(E).

[11] R.J. Baxter, J. Phys. **C6** (1973) L445; J. Stat. Phys. **9** (1973) 145.

[12] R.J. Baxter, J. Phys. **A15** (1982) 3329.

[13] E. Buffenoir and S. Wallon, J. Phys. **A26** (1993) 3045; A. Klümper, Int. J. Mod. Phys. **B4** (1990) 871; A. Klümper, A. Schadschneider, and J. Zittartz, Z. Phys. **B76** (1989) 247.

[14] C. Borgs and W. Janke, J. Phys. I (France) **2** (1992) 2011.

[15] C.M. Fortuin and P.W. Kasteleyn, Physica **57** (1972) 536; C.M. Fortuin, Physica **58** (1972) 393; *ibid.* **59** (1972) 545; P.W. Kasteleyn and C.M. Fortuin, J. Phys. Soc. Japan **26** (Suppl.) (1969) 11.

[16] W. Janke and S. Kappler, Nucl. Phys. **B** (Proc. Suppl.) **34** (1994) 674.

[17] W. Janke and S. Kappler, Phys. Lett. **A197** (1995) 227.

[18] W. Janke and S. Kappler, Nucl. Phys. **B** (Proc. Suppl.) **42** (1995) 770.

[19] W. Janke and S. Kappler, Europhys. Lett. **31** (1995) 345.

[20] K.M. Briggs, I.G. Enting, and A.J. Guttmann, J. Phys. **A27** (1994) 1503.

Table 1: Integrated autocorrelation time $\tau_{\mathrm{int},e}$ of the energy and the number of Monte Carlo update sweeps (MCS) in units of $\tau_{\mathrm{int},e}$.

	$q = 10$ 300×300	$q = 15$ 120×120	$q = 20$ 80×80
ordered phase (heat-bath algorithm)			
$\tau_{\mathrm{int},e}$	≈ 170	≈ 20	≈ 9
$\mathrm{MCS}/\tau_{\mathrm{int},e}$	60 000	640 000	1 280 000
disordered phase (single-cluster algorithm)			
$\tau_{\mathrm{int},e}$	≈ 59	≈ 18	≈ 25
$\mathrm{MCS}/\tau_{\mathrm{int},e}$	600 000	9 000 000	4 200 000

Table 2: Comparison of numerical and analytical results for energy cumulants at β_t in the disordered phase.

Observable	$q = 10$ $L = 150$	$q = 15$ $L = 60$	$q = 20$ $L = 40$
e_d $(d, \ L \times \ L)$	$-0.96812(15)$	$-0.75053(13)$	$-0.62648(20)$
e_d $(d, 2L \times \ L)$	$-0.968190(81)$	$-0.750510(65)$	$-0.626555(97)$
e_d $(d, 2L \times 2L)$	$-0.968186(18)$	$-0.7504949(73)$	$-0.626519(13)$
e_d (exact)	$-0.968203...$	$-0.750492...$	$-0.626529...$
c_d $(d, \ L \times \ L)$	18.33(17)	8.695(47)	6.144(43)
c_d $(d, 2L \times \ L)$	18.34(12)	8.665(29)	6.140(27)
c_d $(d, 2L \times 2L)$	18.437(40)	8.6507(57)	6.1327(38)
c_d (large q)	18.43(2)	8.657(3)	6.1326(4)
$\mu_d^{(3)}$ $(d, \ L \times \ L)$	$-2010(100)$	$-171.0(5.1)$	$-54.7(1.9)$
$\mu_d^{(3)}$ $(d, 2L \times \ L)$	$-2031(73)$	$-176.1(3.8)$	$-53.9(1.5)$
$\mu_d^{(3)}$ $(d, 2L \times 2L)$	$-2015(26)$	$-176.01(76)$	$-54.85(29)$
$\mu_d^{(3)}$ (large q)	$-1834(200)$	$-174(4)$	$-54.7(4)$

Table 3: Comparison of numerical and analytical results for energy cumulants at β_t in the ordered phase.

Observable	$q = 10$ $L = 150$	$q = 15$ $L = 60$	$q = 20$ $L = 40$
e_o $(o,\ L \times\ L)$	$-1.664177(81)$	$-1.765850(34)$	$-1.820722(43)$
e_o $(o, 2L \times\ L)$	$-1.664262(57)$	$-1.765875(26)$	$-1.820689(14)$
e_o $(o, 2L \times 2L)$	$-1.664224(58)$	$-1.765914(27)$	$-1.820659(20)$
e_o (exact)	$-1.664253...$	$-1.765906...$	$-1.820684...$
c_o $(o,\ L \times\ L)$	17.95(13)	8.016(21)	5.351(15)
c_o $(d,\ L \times\ L)$	17.88(17)	8.037(47)	5.373(43)
c_o $(o, 2L \times\ L)$	17.81(10)	8.004(19)	5.3612(55)
c_o $(d, 2L \times\ L)$	17.89(12)	8.007(29)	5.369(27)
c_o $(o, 2L \times 2L)$	18.00(10)	7.990(19)	5.3608(88)
c_o $(d, 2L \times 2L)$	17.989(40)	7.9931(57)	5.3613(38)
c_o (large q)	17.98(2)	7.999(3)	5.3612(4)
$\mu_o^{(3)}$ $(o,\ L \times\ L)$	1979(87)	180.5(3.1)	57.0(1.3)
$\mu_o^{(3)}$ $(d,\ L \times\ L)$	2026(100)	175.7(5.1)	56.9(1.9)
$\mu_o^{(3)}$ $(o, 2L \times\ L)$	1836(71)	189.7(5.1)	56.24(40)
$\mu_o^{(3)}$ $(d, 2L \times\ L)$	2047(73)	180.8(3.8)	56.1(1.5)
$\mu_o^{(3)}$ $(o, 2L \times 2L)$	2030(110)	177.2(3.2)	56.83(71)
$\mu_o^{(3)}$ $(d, 2L \times 2L)$	2031(26)	180.67(76)	57.09(29)
$\mu_o^{(3)}$ (large q)	1900(200)	179(4)	56.9(4)

Table 4: Numerical estimates of higher-order energy cumulants in the disordered and ordered phase at β_t.

Observable	$q = 10$ $L = 150$	$q = 15$ $L = 60$	$q = 20$ $L = 40$
$\kappa_d^{(4)}$ $(d, 2L \times L)$	$1.61(14) \times 10^6$	$3.07(24) \times 10^4$	$4.87(38) \times 10^3$
$\kappa_d^{(4)}$ $(d, 2L \times 2L)$	$1.583(64) \times 10^6$	$3.193(48) \times 10^4$	$4.905(89) \times 10^3$
$\kappa_o^{(4)}$ $(o, 2L \times L)$	$1.10(13) \times 10^6$	$3.95(47) \times 10^4$	$4.67(14) \times 10^3$
$\kappa_o^{(4)}$ $(o, 2L \times 2L)$	$1.55(22) \times 10^6$	$2.93(20) \times 10^4$	$4.79(22) \times 10^3$
$\kappa_o^{(4)}$ (large q)	$1.3(2) \times 10^6$	$3.1(2) \times 10^4$	$5.0(1) \times 10^3$
$\kappa_d^{(5)}$ $(d, 2L \times L)$	$-2.39(39) \times 10^9$	$-1.10(23) \times 10^7$	$-8.1(1.1) \times 10^5$
$\kappa_d^{(5)}$ $(d, 2L \times 2L)$	$-2.40(26) \times 10^9$	$-1.170(59) \times 10^7$	$-8.42(32) \times 10^5$
$\kappa_o^{(5)}$ $(o, 2L \times L)$	$1.03(25) \times 10^9$	$1.73(49) \times 10^7$	$7.16(65) \times 10^5$
$\kappa_o^{(5)}$ $(o, 2L \times 2L)$	$1.98(51) \times 10^9$	$0.92(15) \times 10^7$	$7.37(70) \times 10^5$
$\kappa_o^{(5)}$ (large q)	$\approx 10^9$	$\approx 10^7$	$\approx 10^6$
$\kappa_d^{(6)}$ $(d, 2L \times L)$	$5.1(1.2) \times 10^{12}$	$6.6(2.7) \times 10^9$	$1.77(34) \times 10^8$
$\kappa_d^{(6)}$ $(d, 2L \times 2L)$	$5.8(1.3) \times 10^{12}$	$7.2(1.1) \times 10^9$	$2.33(16) \times 10^8$
$\kappa_o^{(6)}$ $(o, 2L \times L)$	$1.13(48) \times 10^{12}$	$11.9(5.4) \times 10^9$	$1.63(36) \times 10^8$
$\kappa_o^{(6)}$ $(o, 2L \times 2L)$	$2.8(1.4) \times 10^{12}$	$4.5(1.3) \times 10^9$	$1.38(26) \times 10^8$
$\kappa_o^{(6)}$ (large q)	$\approx 10^{12}$	$\approx 3 \times 10^9$	$\approx 2 \times 10^8$
$\kappa_d^{(7)}$ $(d, 2L \times L)$	$-1.20(39) \times 10^{16}$	$-5.5(3.5) \times 10^{12}$	$-4.0(1.1) \times 10^{10}$
$\kappa_d^{(7)}$ $(d, 2L \times 2L)$	$-2.01(66) \times 10^{16}$	$-6.8(2.1) \times 10^{12}$	$-8.47(96) \times 10^{10}$
$\kappa_o^{(7)}$ $(o, 2L \times L)$	$1.15(92) \times 10^{15}$	$1.03(60) \times 10^{13}$	$5.0(2.2) \times 10^{10}$
$\kappa_o^{(7)}$ $(o, 2L \times 2L)$	$3.9(4.2) \times 10^{15}$	$3.0(1.2) \times 10^{12}$	$2.6(1.0) \times 10^{10}$
$\kappa_d^{(8)}$ $(d, 2L \times L)$	$2.9(1.3) \times 10^{19}$	$5.5(4.4) \times 10^{15}$	$7.9(3.7) \times 10^{12}$
$\kappa_d^{(8)}$ $(d, 2L \times 2L)$	$8.6(3.5) \times 10^{19}$	$8.8(4.4) \times 10^{15}$	$3.57(56) \times 10^{13}$
$\kappa_o^{(8)}$ $(o, 2L \times L)$	$\approx 1 \times 10^{17}$	$1.01(69) \times 10^{16}$	$2.0(1.3) \times 10^{13}$
$\kappa_o^{(8)}$ $(o, 2L \times 2L)$	$\approx -2 \times 10^{15}$	$2.1(1.1) \times 10^{15}$	$3.1(4.2) \times 10^{12}$

Table 5: The magnetic susceptibility χ_d at β_t in the disordered phase using different estimators.

Lattice	Observable	$q = 10$ $L = 150$	$q = 15$ $L = 60$	$q = 20$ $L = 40$
$L \times L$	$\frac{q}{(q-1)^2} \sum_{i=1}^{L} g(i)$	4.224(16)	0.7306(14)	0.3092(58)
	$\frac{1}{q-1}\langle \lvert C \rvert^2 \rangle_{d,\mathrm{SW}} / \langle \lvert C \rvert \rangle_{d,\mathrm{SW}}$	4.224(16)	0.7306(14)	0.3092(58)
	$\frac{1}{q-1}\langle \lvert C \rvert \rangle_{d,\mathrm{SC}}$	4.224(16)	0.7310(14)	0.3090(58)
$2L \times L$	$\frac{q}{(q-1)^2} \sum_{i=1}^{2L} g(i)$	4.2306(89)	0.73093(68)	0.30954(32)
	$\frac{1}{q-1}\langle \lvert C \rvert^2 \rangle_{d,\mathrm{SW}} / \langle \lvert C \rvert \rangle_{d,\mathrm{SW}}$	4.2306(89)	0.73093(68)	0.30954(32)
	$\frac{1}{q-1}\langle \lvert C \rvert \rangle_{d,\mathrm{SC}}$	4.2327(89)	0.73094(65)	0.30952(31)
$2L \times 2L$	$\frac{q}{(q-1)^2} \sum_{i=1}^{2L} g(i)$	4.2326(18)	0.730386(79)	0.309356(39)
	$\frac{1}{q-1}\langle \lvert C \rvert^2 \rangle_{d,\mathrm{SW}} / \langle \lvert C \rvert \rangle_{d,\mathrm{SW}}$	4.2326(18)	0.730386(79)	0.309356(39)

Table 6: The magnetization m and m' at β_t in the ordered phase, using the two estimators $M_{\max}$ and $M_{\rm clus}$, and the corresponding susceptibilities and third moments.

Observable	$q = 10$ $L = 150$	$q = 15$ $L = 60$	$q = 20$ $L = 40$
m $(L \times L)$	0.857047(71)	0.916631(21)	0.941199(21)
m' $(L \times L)$	0.857047(71)	0.916634(21)	0.941197(21)
m $(2L \times L)$	0.857113(49)	0.916648(16)	0.9411782(66)
m' $(2L \times L)$	0.857113(49)	0.916648(16)	0.9411791(66)
m $(2L \times 2L)$	0.857081(49)	0.916672(15)	0.9411694(97)
m' $(2L \times 2L)$	0.857077(49)	0.916672(15)	0.9411694(97)
m (exact)	0.857106...	0.916663...	0.9411759...
χ_o $(L \times L)$	4.750(60)	0.8090(36)	0.3348(17)
χ'_o $(L \times L)$	4.704(60)	0.7989(36)	0.3305(17)
χ_o $(2L \times L)$	4.663(43)	0.8095(38)	0.33509(55)
χ'_o $(2L \times L)$	4.623(43)	0.7997(38)	0.33076(55)
χ_o $(2L \times 2L)$	4.744(42)	0.8052(28)	0.33551(81)
χ'_o $(2L \times 2L)$	4.700(43)	0.7953(28)	0.33118(80)
$m_o^{(3)}$ $(L \times L)$	$-1521(85)$	$-45.9(1.2)$	$-8.55(32)$
$m_o'^{(3)}$ $(L \times L)$	$-1505(84)$	$-45.4(1.2)$	$-8.44(32)$
$m_o^{(3)}$ $(2L \times L)$	$-1372(62)$	$-49.4(2.2)$	$-8.321(88)$
$m_o'^{(3)}$ $(2L \times L)$	$-1362(62)$	$-48.9(2.2)$	$-8.216(88)$
$m_o^{(3)}$ $(2L \times 2L)$	$-1532(74)$	$-45.3(1.0)$	$-8.44(13)$
$m_o'^{(3)}$ $(2L \times 2L)$	$-1517(75)$	$-44.8(1.0)$	$-8.33(13)$

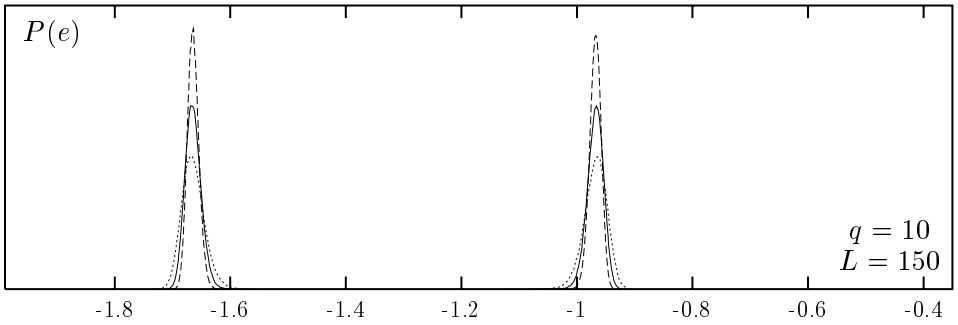

Figure 1: The energy probability distribution $P(e)$ of the 10-state model at β_t in the ordered and disordered phase for $L \times L$ (dotted lines), $2L \times L$ (solid lines), and $2L \times 2L$ (dashed lines) lattices. The area under each peak is normalized to unity.

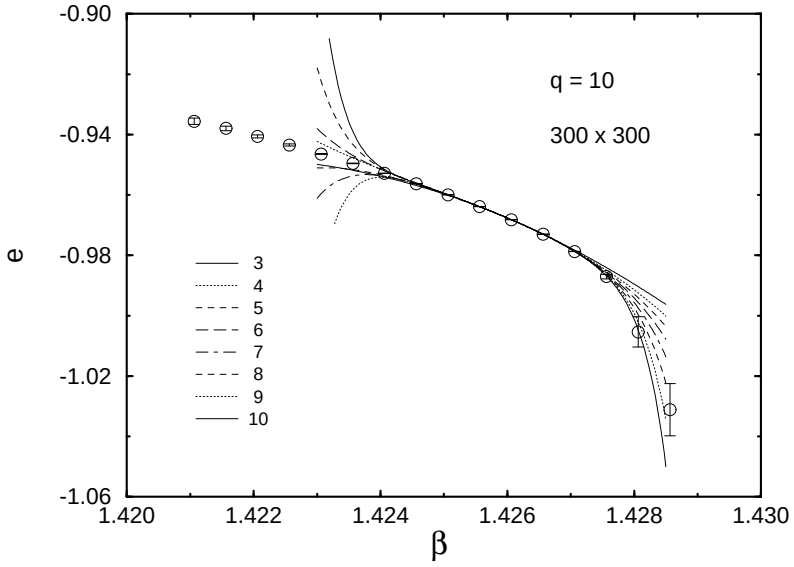

Figure 2: Cumulant expansion of the energy density $e = -(d/d\beta)(-\beta f)$ for $q = 10$ around $\beta_t = \log(1 + \sqrt{10}) \approx 1.426\,062\ldots$ in the disordered phase. The numbers $n = 3, 4, 5, \ldots$ in the legend indicate the highest order of the cumulants $\kappa_d^{(n)}$ involved in the expansion. The open circles show for comparison the energy as obtained by standard reweighting.